



Photon Conversion Efficiency at CDF

Paola Ruggiero, University of Pisa, Italy

September 28, 2013

Abstract

Cdf has never had a program whose goal was a systematic study and understanding of the efficiency for reconstruction of photon detection through the conversion process. Here a first attempt is proposed: the conversion reconstruction efficiency has been extracted from the data, focusing on the process $D_0^* \rightarrow D_0\gamma$ and then basing its overall scale on another well measured quantity: the decay of the charged $D^* \rightarrow D_0\pi$.

Contents

1	Introduction	3
2	The CDF detector	4
3	How does the analysis process work?	6
3.1	Different analysis levels	6
3.2	Conversion algorithm	6
4	Data and Simulation	8
4.1	Data Set	8
4.2	Simulations samples	8
5	Theoretical Approach	9
5.1	D^* s decays	9
5.2	Main goal	9
5.3	Efficiency ratio	10
5.4	Photon efficiency	11
6	Fitting techniques	12
6.1	Models for signal	12
6.2	Models for background	12
6.3	Neutral process: cuts and fit outcomes	13
6.4	Charged process: cuts and fit outcomes	15
7	First Method	17
7.1	Results for conversion efficiency	17
8	Second Method	18
8.1	Simulation of conversion process	18
8.2	Checks on acceptance	18
8.2.1	Check from Distribution of the Electron energy fraction	18
8.2.2	Check from simulated photons	20
8.3	Results for conversion efficiency	21
9	Sources of error and fixed results	22
9.1	Distribution of the D^* decay angle	22
9.2	Isospin invariant assumption	24
9.3	Final result for Photon Efficiency	24
10	Conclusions	25

1 Introduction

The aim of this project is the study of the photon conversion efficiency at CDF. This method gives the most precise measure of photon momentum, whereas calorimetric methods are much less precise and also tend to suffer from large background, due to the presence of different mechanisms for soft photon production in hadron collisions ($\pi_0 \rightarrow \gamma\gamma$, etc). However the technique of reconstruction on photons from the conversion process is fairly inefficient because of the detector acceptance (CDF detector only store tracks with transverse momentum greater than 0.4 GeV), and therefore the measurements suffer from a small sample size and are statistically limited.

The understanding of the performances of the CDF detector for the conversion is important for a variety of physics measurements involving electromagnetic decay products. First because the position distributions of conversion candidates can be used to estimate the distribution and quantity of material within the detector itself. And the uniform tube, at 40 cm, that is 1% of a radiation length thick, is a very important and clear reference to understand how much the simulations still need to be fixed in order to look like data.

Another important reason to look at the conversion efficiency is its application to the $\chi_{c1,2}$ reconstruction: in fact, even if this efficiency will always be low, this technique of photon reconstruction has the precision of the tracking system, allowing the reconstruction of the charmonium states through the decay $\chi_{c1,2} \rightarrow J/\psi - \gamma$, and giving a mass resolution sufficient to separate the $\chi_1(3510)$ from the $\chi_2(3555)$.

In this report, after an overview of how the analysis process works at CDF, including in particular a short description of the algorithm used for conversion reconstruction, we will illustrate the main idea of this project and how we implemented it in some details. Then we will point out the techniques used, showing fitting methods and the choices made for cuts. And we'll come to discuss some results, trying to draw a conclusion from them.

2 The CDF detector

The Collider Detector at Fermilab (CDF) experimental collaboration is committed to studying high energy particle collisions at the worlds highest energy proton-antiproton collider.

The goal is to discover the identity and properties of the particles that make up the universe and to understand the forces and interactions between those particles.

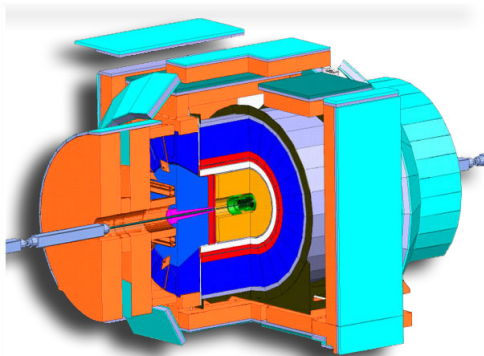


Figure 1: *The CDF detector*

The CDF detector is designed in many different layers:

- **Beam Pipe:** where the protons and anti-protons collide head on.
- **Silicon Detector:** This detector is used to track the path of charged particles as they travel through the detector. It begins at a radius of $r = 1.5$ cm from the beam line and extends to a radius of $r = 40$ cm from the beam line. The silicon detector is composed of seven layers of silicon arranged in a barrel shape around the beam pipe. Silicon is often used in charged particle detectors because of its high sensitivity, allowing for high-resolution vertex and tracking.
- **Central Outer Tracker (COT):** It is also used to track the paths of charged particles and is also located within a magnetic field. The COT, however, is not made of silicon. Silicon is tremendously expensive and is not practical to purchase in extreme quantities. COT is a gas chamber filled with tens of thousands of gold wires arranged in layers and argon gas. Two types of wires are used in the COT: sense wires and field wires. Sense wires are thinner and attract the electrons that are released by the argon gas as it is ionized. The field wires are thicker than the sense wires and attract the positive ions formed from the release of electrons.
- **Solenoid Magnet:** The purpose of the solenoid is to bend the trajectory of charged particles in the COT and silicon detector by creating a magnetic field parallel to the beam. The solenoid has a radius of $r=1.5$ m and is 4.8m in length.

- **Electromagnetic Calorimeters:** It uses alternating sheets of lead and scintillator. Each layer of lead is approximately $3/4$ in wide.
- **Hadronic Calorimeters:** This calorimeter uses steel in place of lead.
- **Muon Detectors** There are two aspects of the muon detectors: the planar drift chambers and scintillators. There are four layers of planar drift chambers, each with the capability of detecting muons with a transverse momentum $p_T > 1.4\text{GeV}/c$.

3 How does the analysis process work?

3.1 Different analysis levels

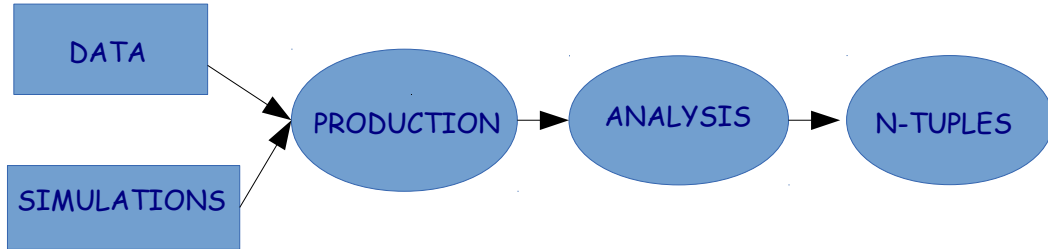


Figure 2: *Different analysis levels*

This section shortly outlines the path from the accelerator collisions to the generated ROOT ntuples. Detector information is gathered during collisions (online), processed later in a computer farm (offline), then run through a user-specific program. The results of that program are in a ROOT file, which is used to generate the final plots.

As we can see from the diagram, after data recording, the first level is the *PRODUCTION*: it is made in such a way that it will work with both data and simulation as input, so that they're treated in the exact same way. At this level all tracks are reconstructed, but with no more specification.

At a higher level there is the *ANALYSIS* program, where a first stage association is made: the selection is here based on requirements on good fit or mass ranges, for example, but not strict ones.

All the information from the *ANALYSIS* level is then stored into N-Tuples, ready to be used for further analysis.

Our project of analysis will work on this *N-TUPLES* level, adding more specific requirements and cuts on these stored variables.

3.2 Conversion algorithm

At the *ANALYSIS* level, a method for conversion identification is implemented. Since our results of course will depend on how good we are at making this identification, it's useful to describe the algorithm used.

The following requirements are used to select photon candidates:

- a loop over oppositely charged tracks is made, with e^+, e^- mass assignments;
- the tracks with a p_T above $400 \text{ MeV}/c$ are checked for intersection: they are required to come within:
 - 2.0 cm in the transverse view
 - 10 cm in the R-Z view;
- track pairs are considered further if their invariant mass is found to be less than $100 \text{ MeV}/c^2$;
- all pairs that have survived these selections are then refit with vertex and pointing constraints. The tracks are required to:
 - be *parallel*: this is an explicit “mass zero ” constraint
 - have an *intersection*;
- Neutral vertex candidates are then saved for further study if the probability of good fit is greater than 10^{-4} .

4 Data and Simulation

4.1 Data Set

More data could be processed, but to start with, we chose to only process 4 periods, from 14 to 17 (out of 38) of the *xbbd0k* data set.

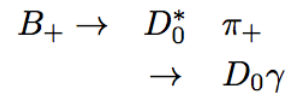
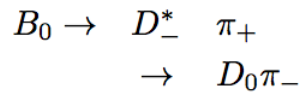
This is just a small sample of all the available data set.

4.2 Simulations samples

We generated two different samples, with the same number of events.

The neutral D^* were generated from the decay $B^+ \rightarrow D_0^* \pi^+$, whereas the charged ones from the process $B_0 \rightarrow D_+^* \pi_-$.

To simulate these decays, the standard event generator used for B-decays is invoked and then the D^* s are allowed to decay naturally according to the PDG listings.



5 Theoretical Approach

5.1 D^* s decays

In order to deduce the photon conversion efficiency, we focused on the decays of the D^* (the first excited state of the D mesons, that are the lightest particles containing charm quarks):

- $D^{*0} \rightarrow D_0 \gamma$
- $D^{*\pm} \rightarrow D_0 \pi$

Why did we choose this two particular decays? What matters for our purposes is that the D^{*0} and the $D^{*\pm}$ belong to the same isospin multiplet. In fact because of the isospin symmetry we expect them to be produced in equal number (*isospin invariant production*) and this will be crucial for our method.

But in comparing these two decays, we also need to take in mind the differences between these 2 processes: in fact, first of all, they are both 2 body decays but the kinematics looks a bit different since in the charged process the pion will be very “soft”, while the photon energy will vary more (it has no mass), so that we cannot simply compare the final state of this two particles.

Then a further difference is that the D^*_\pm decay is very common (the branching ratio is about 67,7%) and it's easy to trigger, requiring:

- two tracks with transverse momentum higher than 2 GeV to detect the $D_0 \rightarrow K \pi$
- a track almost parallel to the D_0 one for the other pion (because of its low energy).

Instead the neutral process is rarer, and this is not really because of the branching ratio, that is still quite high (about 38 %), but especially because of conversion: the point is that we will not see all the events where the photon do not convert, and even if it does, we will see the tracks of electron and positron from pair production according to the detector acceptance and efficiency. So this time the requirements are:

- again two tracks with p_T higher than 2.0 GeV to detect the D_0
- two more tracks with p_T higher than 0.4 GeV (e^+, e^-)

5.2 Main goal

The main goal of this project is to understand whether the following expression can be used to obtain the conversion efficiency:

$$1 = \frac{\sigma_{D^*(2007)}}{\sigma_{D^*(2010)}} = \frac{N_{D^*(2007)} \epsilon_{D^*(2010)}}{N_{D^*(2010)} \epsilon_{D^*(2007)}} \quad (1)$$

where:

- the first ratio is the one of the cross-sections for the two processes;
- we rewrote this ratio as the ratio of the number of candidates (N), the neutral over the charged ones, calculated from **data**;
- the ratio of the candidates need to be corrected through the efficiency ratio (ϵ) derived instead from **simulations**;

and there is an **assumption**: isospin invariant production of the two different isospin D^* states, that is why the ratio of the cross sections is imposed to be 1.

We expect the efficiency and yields to be strong functions of transverse momentum, angles (η) and other kinematics variables, but for this analysis we focused only on **transverse momentum**: we first bin our sample of D^* in 3 different $p_T(D^*)$ ranges and then, in the neutral process case, for each $p_T(D_0^*)$ bin, we split it again into 3 more $p_T(\gamma)$ bins. This will allow to study the conversion efficiency as a function of $p_T(\gamma)$.

5.3 Efficiency ratio

In equation (1) we have the ratio of efficiencies that should take into account a correction of what we see in real data. How did we deduce it from simulations?

Its meaning can be better understood if we explicit it:

$$\frac{\epsilon_{D^{*\pm}}}{\epsilon_{D^{*0}}} = \frac{\cancel{\epsilon(D^{*0})}}{\cancel{\epsilon(D^{*0})}} \quad \frac{\epsilon_\pi}{\epsilon_\gamma} = \frac{N(D^{*-} \rightarrow D^0 \pi^-_{[reco]})}{N(D^{*0} \rightarrow D^0 \gamma_{[reco]})} = \frac{N(D^{*-} \rightarrow D^0 \pi^-_{[reco]})}{N(D^{*0} \rightarrow D^0 \gamma_{[gen]}) \epsilon(\gamma)} \quad (2)$$

So what we did was to rewrite the efficiency for D^* as the product of the D_0 and the other final state particle ones, so that the efficiency of D_0 is the same for the 2 processes and cancels out and we only have the ratio of the pion over the photon efficiency. And this is calculated as the number of reconstructed pion (equal of course to the number of $D^{*\pm}$) over the number of reconstructed photons (that is the number of reconstructed D^{*0}).

When we talk about reconstructed events from simulation, what we mean is that we selected our “good events” analysing our simulated events with the same program used for real data selection.

The parameter $\epsilon(\gamma)$ ¹(the unknown parameter we want to derive from this analysis) finally appear by replacing the reconstructed photons with all the generated ones: the power of our method is that it allows to take all the fake photons we generated, and this is crucial since we do not have a big sample for reconstructed D^{*0} .

¹whose meaning will be clarified in the next sections.

5.4 Photon efficiency

Now, depending on the selection made on this set of all generated photons, the parameter $\epsilon(\gamma)$ will turn out to have a different meaning.

Here two versions have been considered.

1st Method : In the first method the simplest choice has been implemented: we just select all the photons generated from the decay of the D^{*0} : this corresponds to consider both acceptance and efficiency to be 100%. In this way, our parameter will be the product of the reconstruction efficiency and the conversion one, and will also include a term of acceptance, A :

$$\epsilon(\gamma) = \epsilon_{Reco} * \epsilon_{Conv} * A. \quad (3)$$

2nd Method : In the second one we also tried to simulate the acceptance of the detector. This means that first, we had to simulate the conversion process (see next sections); after that we selected only the events with the e^+, e^- tracks passing the acceptance requirements ($p_T > 0.4 GeV$) and also a simple efficiency requirement: we used the efficiency function already known for pions², so that we will measure not the reconstruction efficiency itself, but just the correction to this known shape ($\hat{\epsilon}_{Reco}$).

So, with this selection, our parameter $\epsilon(\gamma)$ can be written as the product of two terms (acceptance is already simulated):

$$\epsilon(\gamma) = \hat{\epsilon}_{Reco} * \epsilon_{Conv}. \quad (4)$$

We will not instead be able to divide the contribution of each of his two factors.

²CDF Note 8433

6 Fitting techniques

In order to extract the number of candidates (real data and simulations) from both the processes, we needed to perform some fits.

6.1 Models for signal

For the signals we chose the best fit between 3 different shapes: 1 or 2 gaussians and the so called *crystal ball*.

The last one takes into account the presence of a radiative tail on the low side of the mass, that actually starts to be visible in the histograms of the invariant mass we got for the neutral process, if we do not bin in p_T : presumably, this is due to energy loss of the conversion electrons as they pass through the material of the inner tracker.

So it could reveal to be very useful when processing more data. For our 4-periods data sample the gaussian signal still seemed to fit better, and so we only used the first 2 options.

6.2 Models for background

For the background shape instead, we made different attempts before choosing the same shape for both for the neutral and charged D^* decays:

- *Line*, $ax+b$: it is the simplest one, but it revealed to be enough to fit our simulation characterized by the presence of very small background;
- $a + bx + c\sqrt{x}$
- $x^\alpha e^{-Cx}$: this shape is already implemented for the charged D^{*3} , but appeared to be not very stable for our samples.
- *Polynomial*, $a + bx + bx^2$
- *Modified polynomial*, $aP_0(x) + bP_1(x) + cP_2(x)$: a combinations of the first 3 Chebyshev polynomials (ortogonal and normalized); this shape seemed to give the best fit for our data, and therefore we used this one in order to perform the histograms of the next section.

³CDF Note 7116

6.3 Neutral process: cuts and fit outcomes

In the following histograms the difference of mass $M(D^{*0}) - M(D^0)$ in data is shown, for 3 different range of $p_T(D^{*0})$, each divided into 3 bins of photon transverse momentum. Here below the selection we are using on the events:

- $1.85 \text{ GeV} < D^0 \text{ Mass} < 1.89 \text{ GeV}$
- Impact: $|\text{imp}(D^{*0})| < 0.02 \text{ cm}$ (this is because we want our D^{*0} track to point back to the beam)
- Fit probability: $|\text{P}(D^{*0})| > 1e-4$
- $p_T(\gamma) > 1.0 \text{ GeV}$
- $|\text{Flight}(\gamma)| > 12 \text{ cm}$ (this choice allow to strongly reduce the background, whereas if we cut more the improvement is not significant)

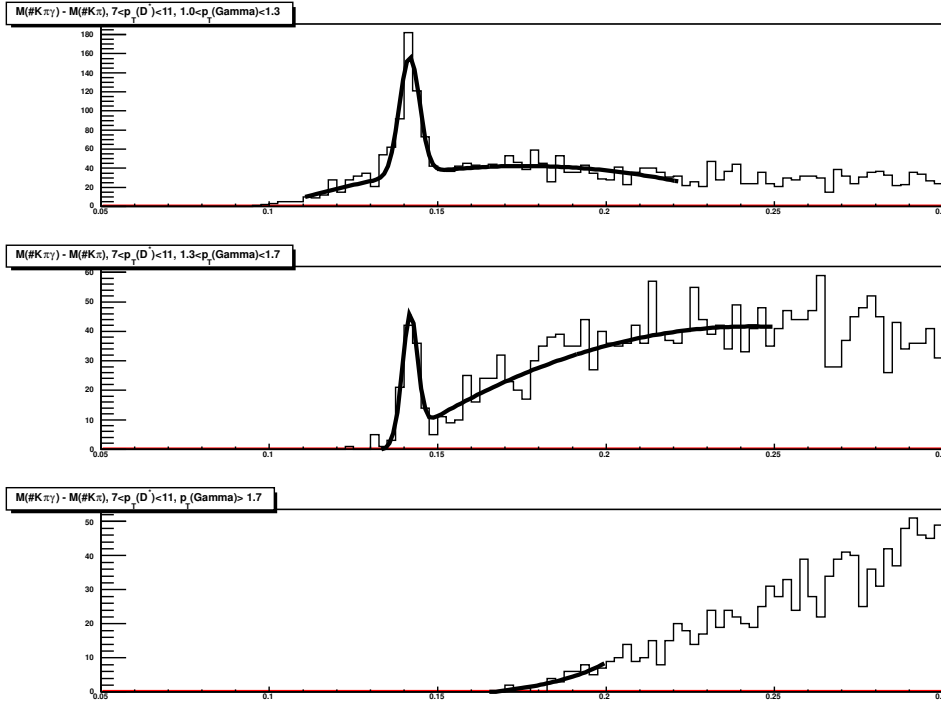


Figure 3: $N(D^{*0} \rightarrow D^0 \gamma_{[reco]}), p_T(D^*) \in [7, 11] \text{ GeV}$ [DATA]

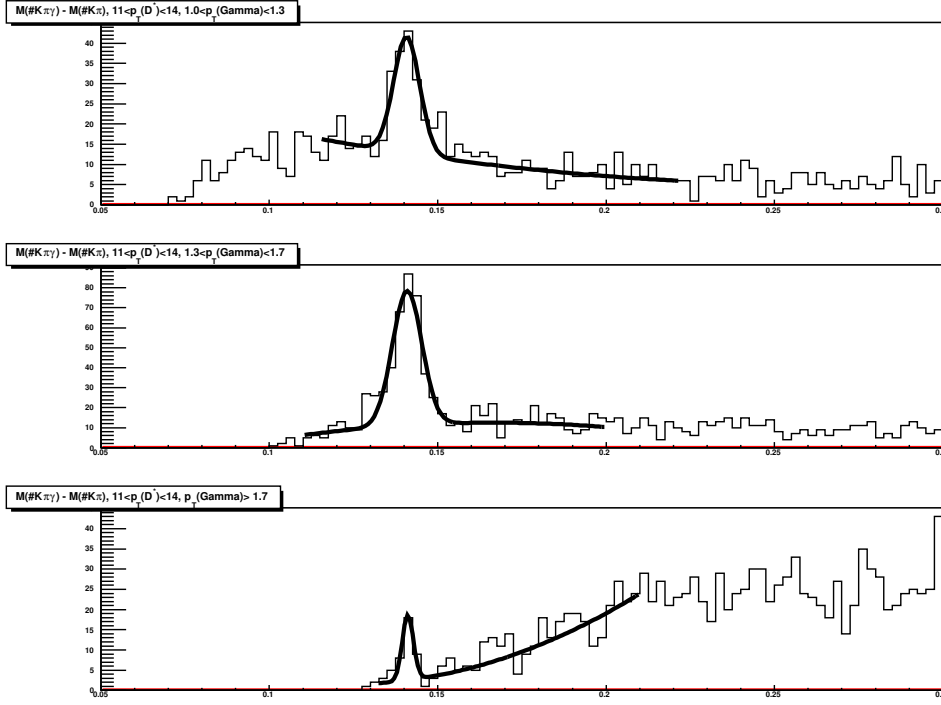


Figure 4: $N(D^{*0} \rightarrow D^0\gamma_{[reco]}), p_T(D^*) \in [11, 14] \text{ GeV}$ [DATA]

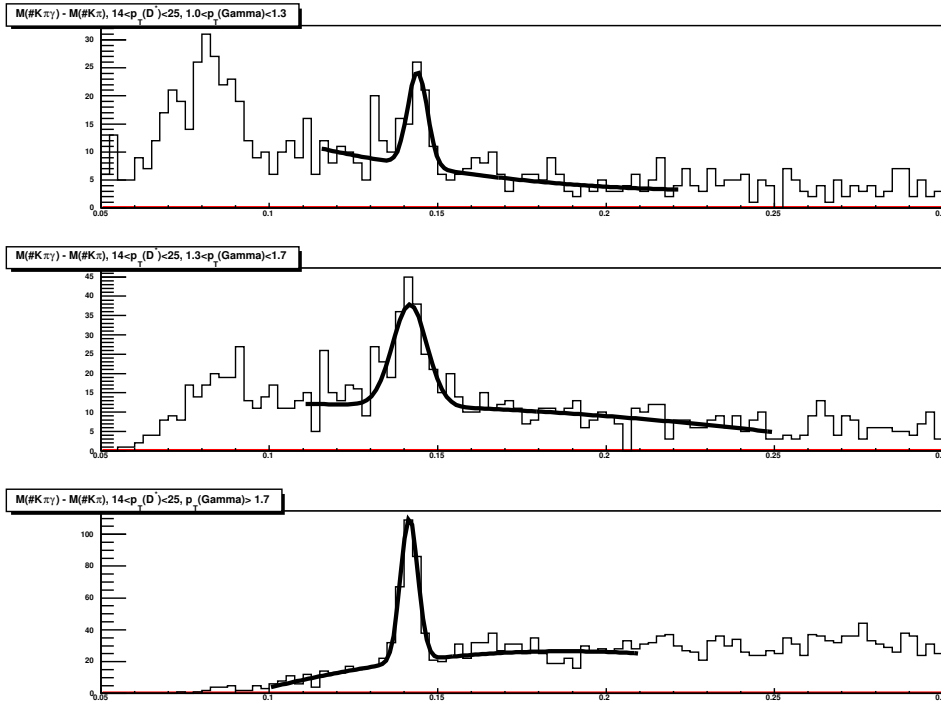


Figure 5: $N(D^{*0} \rightarrow D^0\gamma_{[reco]}), p_T(D^*) \in [14, 25] \text{ GeV}$ [DATA]

What deserves to be mentioned is the pick that at low energy (on the left of the fitted pick), that starts to be visible at high D^* momentum: it is what is usually called “partial reconstruction”, of the π^0 in this case.

The explanation for it is that, as we go up in energy, another relevant channel of decay for the D^{*0} is the $D^0 - \pi^0$ one, with the π^0 immediately decaying to $\gamma - \gamma$. So it can happen for some events that only one of the photons from the π^0 converts: in this case the tracks of the D^0 and this converting photon can be reconstructed as a $D^{*0} \rightarrow D^0 \gamma$ event, but of course this time the photon will be less energetic than expected for our main pick (its energy being roughly half of the pion mass), so that we are able to distinguish the two different contributions.

6.4 Charged process: cuts and fit outcomes

In the following histograms the difference of mass $M(D^*) - M(D_0) - M(\pi)$ for both data and simulations is shown (in this case we only have 3 fit, for our 3 favourite ranges of $p_T(D^{*\pm})$), after a selection using the following cuts:

- $1.85 \text{ GeV} < D_0 \text{ Mass} < 1.89 \text{ GeV}$
- Impact: $|\text{imp}(D^*)| < 0.02 \text{ cm}$
- Fit probability: $|\text{P}(D^*)| > 1\text{e-}4$
- $p_T(\pi) > 0.6 \text{ GeV}$

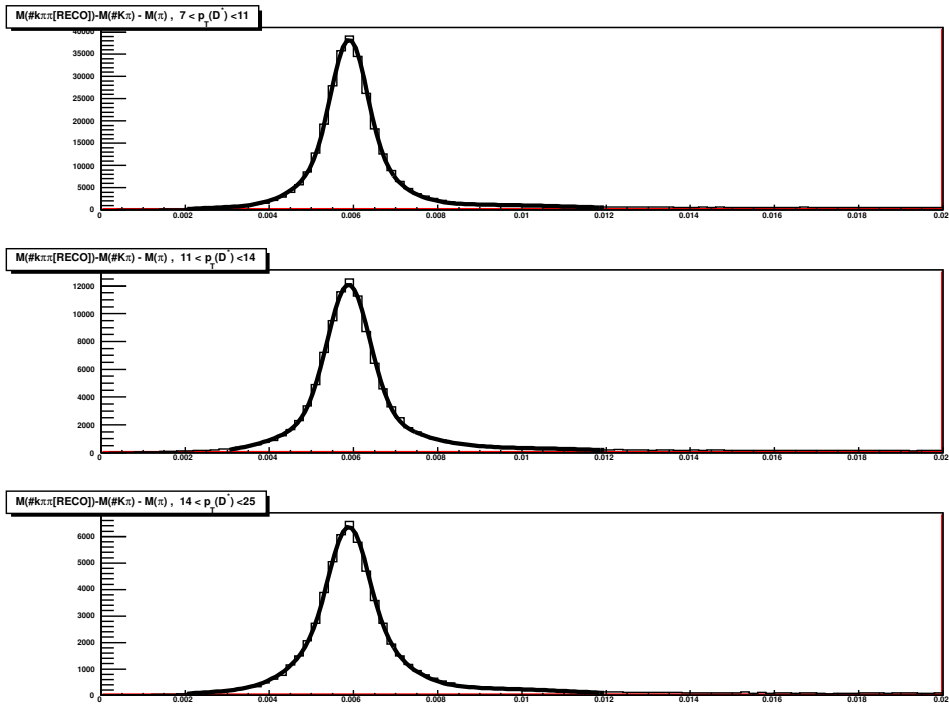


Figure 6: $N(D^* \rightarrow D^0 \pi_{[reco]})$ [DATA]

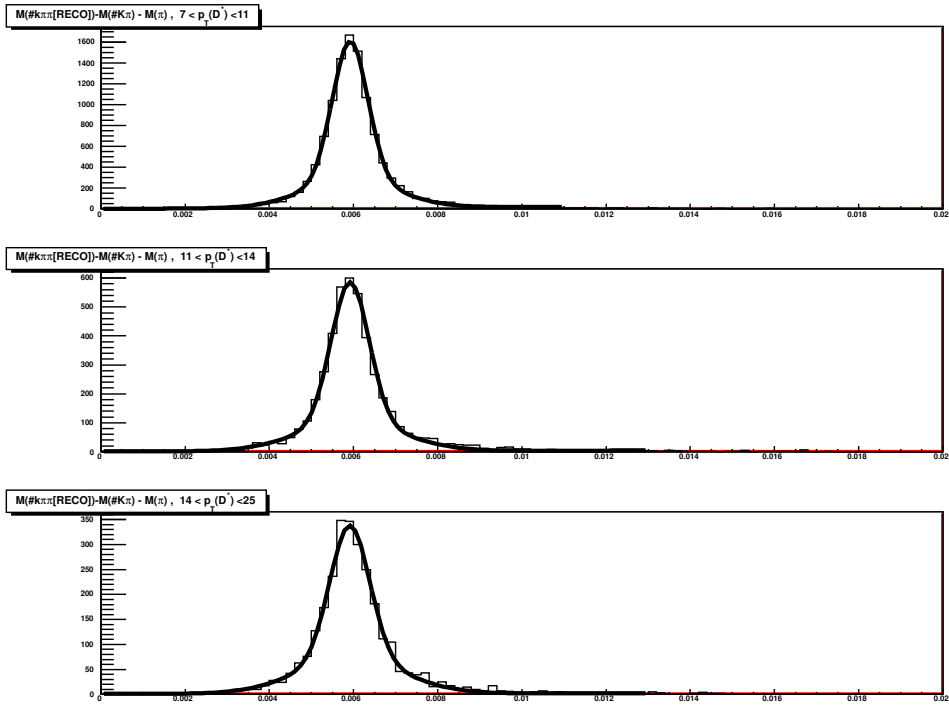


Figure 7: $N(D^* \rightarrow D^0 \pi_{[reco]})$ [SIM]

7 First Method

7.1 Results for conversion efficiency

In the previous section we had no histograms fitting the signal for the number of generated photons, from simulations ($N(D^{*0} \rightarrow D^0 \gamma_{[gen]})$): the reason is that in this case we have no background at all, so that we did not need any fit; instead we just counted the number of events.

In the table below we report the results for the photon conversion efficiency obtained using the second method (no trigger on acceptance):

$p_T(\gamma) \setminus p_T(D^*)$	[7, 11]	[11, 14]	[14, 25]
[1.0, 1.3]	0.0077 ± 0.0005	0.0046 ± 0.0008	0.005 ± 0.001
[1.3, 1.7]	0.022 ± 0.003	0.017 ± 0.001	0.011 ± 0.002
> 1.7	0 ± 0	0.024 ± 0.007	0.023 ± 0.002

Table 1: *Conversion efficiency: Results (2nd Method)*

The efficiency raises with $p_T(\gamma)$, that is what we would expect because the acceptance of our detector improve as we go up in energy.

But on the other hand the behaviour of the number we got is not clear as a function of $p_T(D^*)$.

So from here we miss a complete understanding of our results, also because we have no candidates at all for high photon momentum and low D^* momentum.

8 Second Method

In order to better understand our results we implemented a second method to calculate our efficiency.

8.1 Simulation of conversion process

In this case we needed a more specific selection for the generated photons and, in order to implement it, we had to simulate the conversion process.

How did we generate the pair production? What we did is to start from taking all the photons and then the photon energy fraction taken by the electron and positron was generated according to the Rossi's treatment for the Bethe-Heitler conversion (Figure (8)):

$$\Psi(x) \propto [x^2 + (1-x)^2 + \frac{2}{3}x(1-x)] \ln(183Z^{-\frac{1}{3}}) - \frac{1}{9}x(1-x) \quad (5)$$

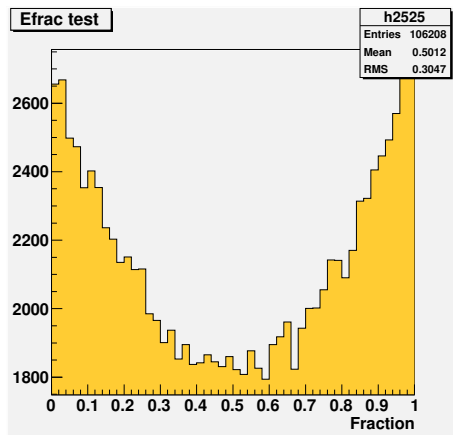


Figure 8: *Electron energy fraction*

This energy fraction is the only information we needed to generate: in fact this is enough to apply the acceptance and efficiency cuts on p_T .

8.2 Checks on acceptance

Before using all this simulated machinery, we made some checks to test it: this will help us to understand if we can trust our simulation of acceptance and in this case we could better use this second method giving us a more specific information, that is the efficiency of reconstruction and conversion, with no dependence on p_T , already included in the acceptance.

8.2.1 Check from Distribution of the Electron energy fraction

A possible non proper simulation of acceptance could be investigated by looking at the distribution of the electron energy fraction.

In the following histograms, the first one is referred to data: as a reference we selected only photons converting at about 40 cm, in the uniform tube, where we can trust the simulation more, so that we know we are looking at real conversions.

Simulations are plotted nearby. The one in the middle shows the simulated fraction, after only the hard cut at 0.4 GeV for the transverse momentum of the e^+, e^- from pair production. In the other one instead we also took into account the correction for the efficiency (the known one for pions we already mentioned), that actually doesn't make a big difference in the shape.

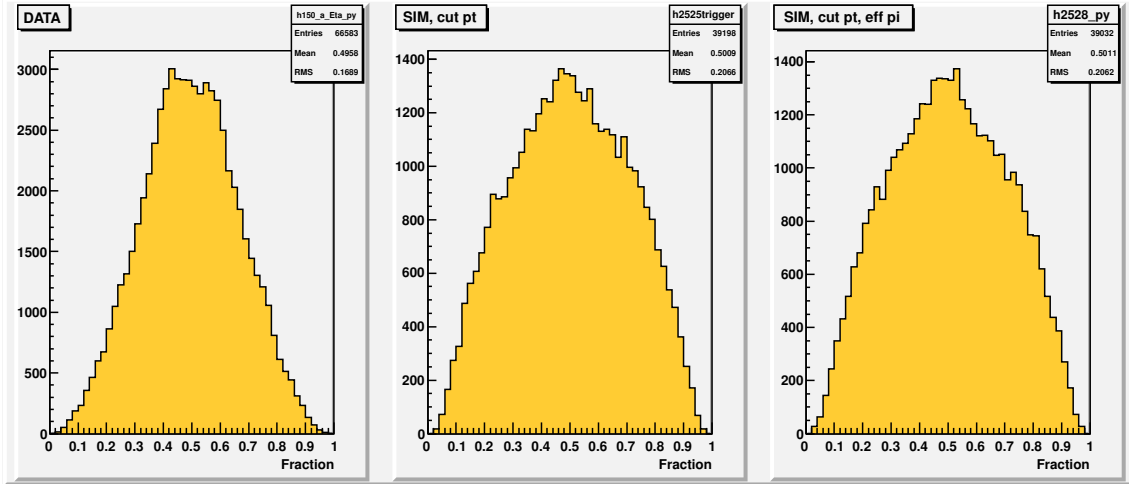


Figure 9: *Electron energy fraction, DATA and SIMULATIONS*

Even if from these overall histograms data and simulations could seem different, investigating more we concluded that this effect is not so important: in fact if instead we slice the energy fraction in our $p_T(\gamma)$ bins, we do not see anymore differences between data and simulation. A small discrepancy only starts to be visible for high energy photons (Figure (12)).

So what we see in Figure (9) is almost the result of the different proportion in distribution of the photon momentum: in simulations photons only come from D^* decays, while in data we are looking to all photons, coming from different sources (such as for example the decay $\pi_0 \rightarrow \gamma\gamma$, in which case the photon in the final state will be less energetic). So this is a first check that tells us that we are simulating the acceptance of the detector in the right way.

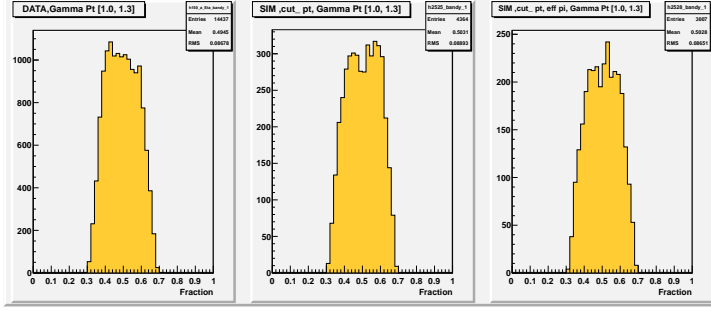


Figure 10: Electron Energy Fraction, $1.0 < p_T(\gamma) \text{ GeV} < 1.3$

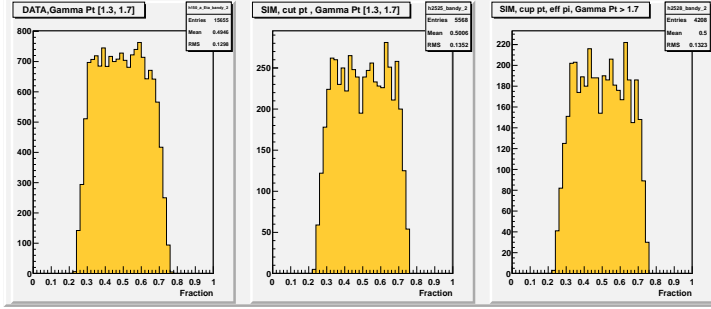


Figure 11: Electron Energy Fraction, $1.3 < p_T(\gamma) \text{ GeV} < 1.7$

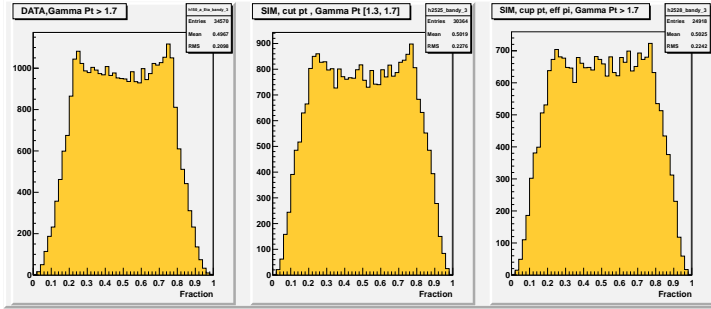


Figure 12: Electron Energy Fraction, $p_T(\gamma) \text{ GeV} > 1.7$

8.2.2 Check from simulated photons

As another check on our acceptance (just looking at simulations this time) for particles from pair production, we also compared the number of reconstructed photons with the generated ones, but after our acceptance and efficient trigger, as a function of $p_T(\gamma)$. We just counted the number of events, having not background.

The results are shown in Table (2).

They show again that we are simulating quite well the real acceptance of the detector: in fact the ratio of our two samples of reconstructed and generated photons remains almost constant.

$p_T(\gamma)$ GeV	$N(\gamma[FAKE])$	$N(\gamma[RECO])$	$\frac{N(\gamma[RECO])}{N(\gamma[FAKE])}$
[1.0, 1.3]	35851 ± 189	3743 ± 61	0.104 ± 0.002
[1.3, 1.7]	47676 ± 218	4874 ± 70	0.102 ± 0.002
[1.7, 2.2]	48252 ± 220	5144 ± 72	0.107 ± 0.001
[2.2, 3.0]	54069 ± 233	5588 ± 75	0.103 ± 0.001
[3.0, 4.0]	40603 ± 202	4420 ± 66	0.109 ± 0.002
[4.0, 5.0]	23667 ± 154	2620 ± 51	0.111 ± 0.002

Table 2: *Acceptance check*

8.3 Results for conversion efficiency

From the previous section we concluded that our simulated acceptance works fine so that we can trust it and use this second method to get our efficiency. Here again, because of the absence of any background we just counted, without any fit, the number of generated photons in each bin.

In the table below we report the results for the efficiency using this alternative method:

$p_T(\gamma) \setminus p_T(D^*)$	[7, 11]	[11, 14]	[14, 25]
[1.0, 1.3]	0.066 ± 0.007	0.042 ± 0.009	0.037 ± 0.009
[1.3, 1.7]	0.13 ± 0.04	0.080 ± 0.009	0.049 ± 0.009
> 1.7	0 ± 0	0.11 ± 0.06	0.072 ± 0.009

Table 3: *Conversion efficiency: Results (1st Method)*

The results we got are not what we would have expected: we expected similar results for photons with the same momentum (the rows), since the reconstruction of photons should have nothing to do with the the particular process we are considering and in particular with the energy of the parent particle. And actually we also expected similar results for different range of $p_T(\gamma)$ since now we are already taking into account the acceptance in the definition of “generated photons”.

Instead what we can noticed is that the efficiency seems to raise with $p_T(\gamma)$ and to fall with $p_T(D^*)$.

A further problem for the understanding of these results is the fact that we have few or no candidates for high photon momentum and low D^* momentum.

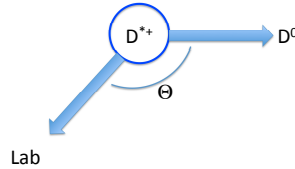
We concluded from here that these results were inconsistent, and for this reason we investigated for possible errors.

9 Sources of error and fixed results

9.1 Distribution of the D^* decay angle

Possible sources of error can be searched into strong differences between simulations and real data.

For example if we look at the distribution of the D^* decay angle (the angle of the D_0 in the D^* frame), we will see big discrepancies between data and simulation samples.



We made this check for the charged D^* first.

In the histograms referred to the charged D^* (Figure (13)), showing the distribution of $\cos(\theta)$, the first one shows real data, the second one is what our original simulations looked like, and the last one show the distribution of the modified simulations we are now using in this analysis.

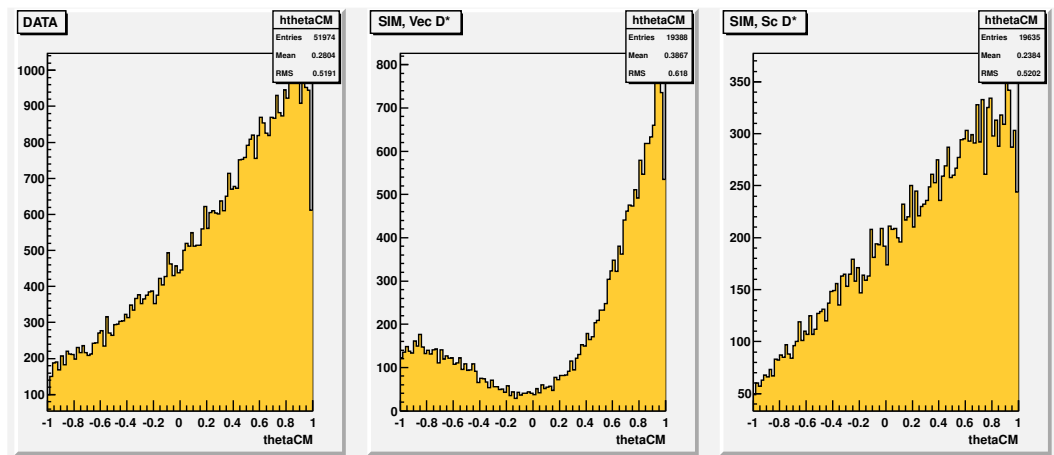
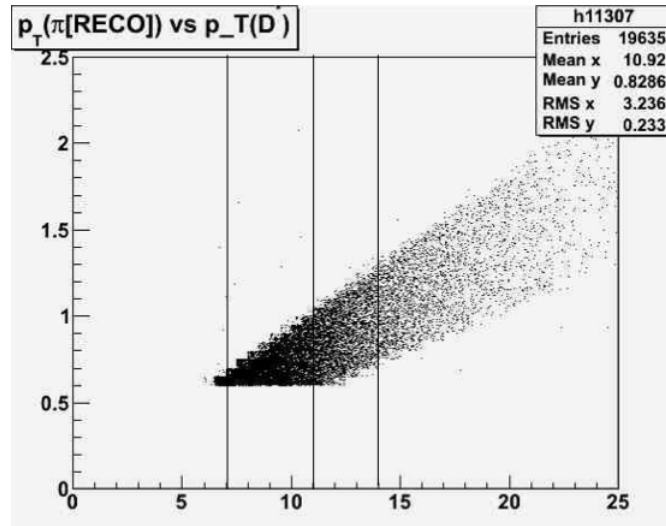


Figure 13: $\cos(\theta)$ distribution, DATA and SIMULATIONS, D^*_{\pm}

The reason for such a different shape is that in data, the D^* s come from many different sources (directly from the beam, from a secondary vertex and so on) and so the distribution will be the results of all these components.

On the contrary, in simulations, for construction, we only have D^* s coming from B -decays: these D^* s will be polarized so that they will decay as spin 1-particles and in fact, as it is clear from the distribution, small angles are preferred (second histogram).

So, as a first, very basic adjustment, we let the D^* 's decay isotropically (third histogram). But, even if it is not clear enough from the figure, our generated sample still look very different from data (data distribution for $\cos(\theta)$ raises faster than the simulated one). How to fix this problem? If we look at the scatter plot of $p_T(\pi)$ versus $p_T(D^{*\pm})$, we can clearly see our hard acceptance cut: we noticed that actually it only affects our first two $p_T(D^*)$ ranges ($[7, 11]GeV$, $[11, 14]GeV$), so that if we focus only on our highest energy range, here we have full acceptance, so that it does not matter anymore the difference in the angular distribution.



Finally the same check was made for the neutral case, but in the last case we don't have a sample large enough (Figure (14)) to draw any conclusion.

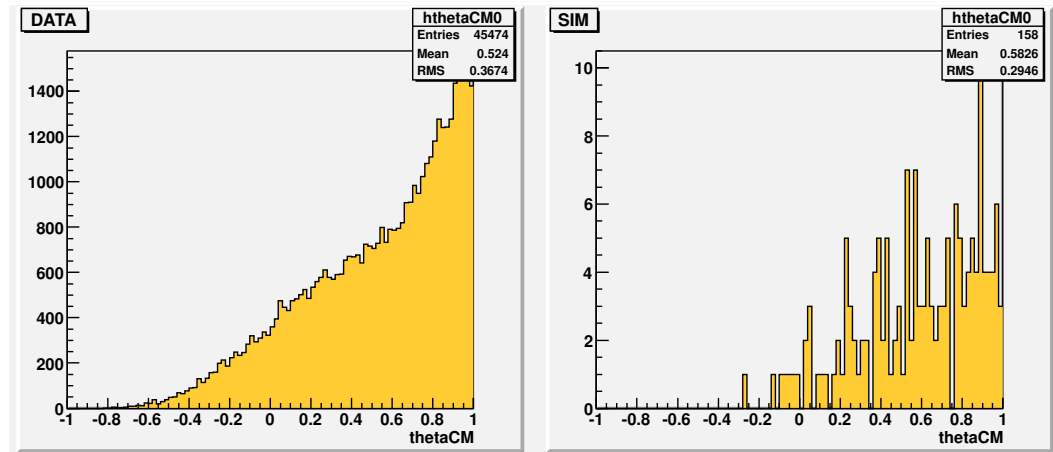


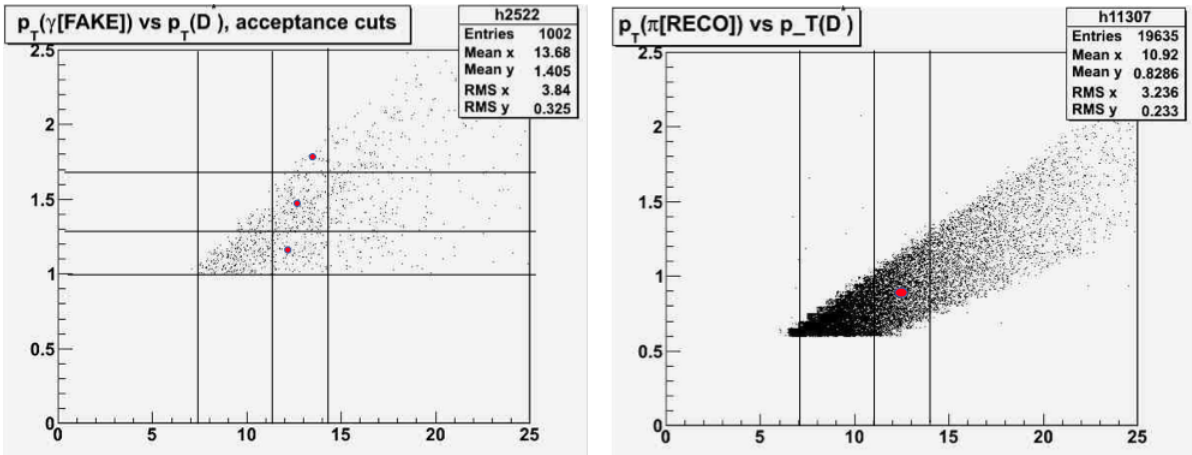
Figure 14: $\cos(\theta)$ distribution, DATA and SIMULATIONS, D_0^*

9.2 Isospin invariant assumption

A mistake we finally found out has instead to do with our method: we are using the assumption of isospin invariant production, and it is for this reason that we are looking at D^* in the same range of transverse momentum. But the point is that, as we can notice from the plots below, there is the correlation between the photon and the D^* momentum, so that because of our binning in photon momentum, we are considering D^* with a different average momentum. In this way it is not satisfied anymore the hypothesis:

$$\langle p_T(D_0^*) \rangle \sim \langle p_T(D_{\pm}^*) \rangle \quad (6)$$

and this means that our assumption of isospin invariance fails.



In order to continue to use it we took a step back, avoiding the additional binning in $p_T(\gamma)$.

9.3 Final result for Photon Efficiency

If we correct for these 2 big problems, we are left with just one range: $p_T(D^*) \in [14, 25] GeV$.

Here we can calculate our efficiency and what we found is:

$$\epsilon(\gamma) = 0.057 \pm 0.004$$

10 Conclusions

Four periods of the *xbhd0k* set of the CDF data has been used to investigate the photon conversion efficiency, reaching a first estimate for it.

What deserves to be mentioned is that this analysis uses the reconstruction of the D^{*0} : this means that we know how to reconstruct this neutral state, that is not very common, the most of the analysis focusing on the charged one.

Of course more work need to be done. In fact so far we found a first reasonable estimate for the conversion efficiency, but it can surely be improved using more data.

Furthermore, we also found issues in simulations that need to be fixed.

And finally, it would be important to remake the same analysis with a different method for comparison: our result in fact is not supposed to depend on the method used and the processes considered.

References

- [1] Analysis of $D_0 - \bar{D}_0$ Mixing in the $K\pi$ Channel, *Mark Mattson, Paul Karchin, CDF Note 8433, August 6, 2004*
- [2] Measurement of the $H_b \rightarrow \mu^+ D_0 X, D_0 \rightarrow K^+ \pi^-$ Cross-section times Branching Fraction , *James Kraus, Kevin Pitts, CDF Note 7116, March 31, 2007*
- [3] A Thchnique for Photon Conversion Detection, Applications for material study and Measurement of the $\chi_{c1,2}$, *Patrick Lukens, CDF Note 2797, August 31, 1994*
- [4] Brief Description of the CDF Detector in Run II, *2004*
- [5] <http://www-cdf.fnal.gov/>
- [6] <http://root.cern.ch/>
- [7] <http://pdg.lbl.gov/>